

Chapter 4

A Human MUTYH Variant Linking Colonic Polyposis to Redox Degradation of the $[4Fe4S]^{2+}$ Cluster

Adapted from: McDonnell, K.J.; Chemler, J.A.; Bartels, P.L.; O'Brien, E.; Marvin, M.L.; Ortega, J.; Stern, R.H.; Raskin, L.; Li, G.; Sherman, D.H.; Barton, J.K.; Gruber, S.B. A Human MUTYH Variant Linking Colonic Polyposis to Redox Degradation of the $[4Fe4S]^{2+}$ Cluster. **2018**, *Submitted*.

P. Bartels carried out all electrochemistry and UV-visible, circular dichroism, and EPR spectroscopy. E. O'Brien assisted with electrochemistry. K. McDonnell and J. Chemler identified the C306W mutation, purified proteins, and carried out characterization of the latter (activity assays, biolayer interferometry, and iron quantification).

Introduction

In cells sustaining oxidative damage, genomic guanine residues may be oxidized to 8-oxo-7,8 dihydroguanine (8-oxoG). Unlike guanine, 8-oxoG can pair effectively with either cytosine or adenine bases, with potentially serious mutagenic consequences (1, 2). A DNA glycosylase conserved among species from bacteria to humans, known in humans as MUTYH, removes adenine from these 8-oxoG:A mispairs as part of the base excision repair pathway. In humans, germline *MUTYH* mutations that impair enzymatic activity lead to an increase in G:C to T:A transversions that have been shown to result in missense mutations in the *APC* tumor suppressor gene. Mutations in *APC* are the first recognizable genetic events that initiate malignant transformation of normal colonic epithelia into polyps, specifically adenomas, prior to the acquisition of other mutations that complete the neoplastic conversion sequence from normal tissue through adenoma to carcinoma (3, 4). Bi-allelic mutations of *MUTYH* give rise to the autosomal recessive cancer genetic syndrome, *MUTYH*-associated polyposis, MAP (5-7). Typically, by their fifth decade, MAP patients develop 10-100 colonic polyps (8-10). *MUTYH* variants are common with a prevalence of at least 1-2% among Western Europeans (11), and the colorectal cancer risk increases nearly 2- and 100-fold for mono- and bi-allelic *MUTYH* mutations, respectively (12, 13).

The MUTYH protein comprises three major regions (14): the N-terminus, which contains the Endonuclease III 6-helix barrel catalytic domain, the interdomain connector (IDC), and the C-terminus, corresponding to protein residues 1-306, 315-366, and 368-500, respectively. The MUTYH N-terminus contains a $[4Fe4S]^{2+}$ cluster ligated by four cysteine residues; though metabolically expensive, the cluster is conserved in MutY homologues across all domains of life (15). A rare exception is the yeast endonuclease III homologue Ntg1, which has no cluster, but

one is present in a second yeast homologue (Ntg2) (16). Indeed, the only organisms lacking a cluster in any MutY homologue are specialized anaerobes subjected to lower levels of oxidative stress (17). Studies performed on *Escherichia coli* MutY and its homologue endonuclease III (EndoIII) have demonstrated that the cluster is unnecessary for structural integrity and is largely redox inert in solution (18, 19). However, when *E. coli* MutY and EndoIII were incubated on duplex DNA-modified gold electrodes, a reversible redox signal centered near 80 mV versus NHE was observed for both proteins and identified as the $[4\text{Fe4S}]^{3+/2+}$ couple, an assignment supported by EPR spectroscopy (20). Subsequent experiments with EndoIII on a graphite electrode in the presence and absence of DNA revealed that binding to the negatively charged DNA backbone shifts the redox potential of these proteins by about -200 mV, activating the cluster toward oxidation and resulting in a significant increase in binding affinity of the oxidized $[4\text{Fe4S}]^{3+}$ form of the enzyme relative to the native $[4\text{Fe4S}]^{2+}$ form (21).

These studies have led to a model in which $[4\text{Fe4S}]$ BER proteins with similar DNA-bound redox potentials use reversible redox exchanges to signal to one another across the genome, taking advantage of the unique ability of DNA to conduct charge across the π -stacked base pairs (bps) in a process known as DNA-mediated charge transport (DNA CT) (22, 23). DNA CT has both a very shallow distance dependence and an exquisite sensitivity to even slight disruptions in base pair stacking, making it an ideal lesion reporter. In our CT signaling model, oxidative stress generates highly reactive species, such as guanine radicals, which can then oxidize proteins including MutY (24). If another $[4\text{Fe4S}]$ protein is bound at a distal site and the intervening DNA is undamaged, it can send an electron through the DNA to reduce the first protein. Upon reduction, the protein's affinity for DNA is decreased and the protein dissociates to another region of the genome, while the oxidized protein remains bound. In the presence of a

lesion, DNA CT is impaired, and the oxidized protein will remain bound and diffuse toward the site of damage. Thus, DNA CT constitutes a means for [4Fe4S] proteins to scan a vast genome on a relevant time scale and redistribute in the vicinity of lesions. In the case of *E. coli*, long-range signaling by DNA CT has been estimated to reduce the damage search time from 45 minutes to 10 minutes or less (25).

In the present study, we describe a novel MUTYH variant, p.C306W, discovered in a patient exhibiting colonic polyposis. This mutant was isolated using an *E. coli* overexpression system along with WT and the well-characterized mutants Y179C and G396D, and electrochemistry, UV-visible and EPR spectroscopy were used to compare the redox properties of these four MUTYH variants. Enzymatic activity and DNA binding parameters were compared using glycosylase assays and biolayer interferometry (BLI), respectively. Together, these results provide strong evidence for a primary function of the [4Fe4S] cluster in DNA-mediated redox signaling and establish MUTYH C306W as a pathogenic variant, enhancing our understanding of the role of the [4Fe4S] cluster in human disease.

Materials and Methods

Determination of Trans Chromosomal Configuration of MUTYH Gene Variants

Germline DNA was amplified using the polymerase chain reaction (PCR) to generate a 935 base pair amplicon that includes the open reading frame positions c.918C>G (p.C306W) and c.1187G>A (p.G396D). The PCR reaction used the forward primer 5'-CCA GGA GAT TTC AAC CAA GC-3' and the reverse primer 5' -AAG GGT CAA GGG GTT CAA AT-3'. The c.1187G>A mutation creates a unique BglII restriction endonuclease site which allowed generation of a 719 base pair fragment from the parent 935 base pair amplicon. The shorter 719 base pair fragment was resolved using agarose gel electrophoresis, purified, and its DNA sequence determined (University of Michigan (U-M) Sequencing Core) to establish the identity of the c.918 position.

Identification of APC gene G:C → T:A Transversions

Tumor DNA was extracted from a formalin-fixed, paraffin-embedded colonic adenoma originating from the proband using the RecoverAll Total Nucleic Acid isolation kit (Ambion). A portion of the mutation cluster region of the *APC* gene (26) was amplified using PCR with the forward primer 5'-TGC CAC AGA TAT TCC TTC ATC A-3' and the reverse primer 5'-CAT GGT TTG TCC AGG GCT AT-3'. The PCR product was subsequently sequenced (U-M Sequencing Core).

Cloning of wild type and Mutant MUTYH Expression Plasmids

A plasmid containing the open reading frame for the beta3 isoform of *MUTYH* (NM_001048174.1) was obtained from OriGene (Catalog #: RC201376-OR, Rockville, MD.) and used as a template for the cloning of derivative constructs. Mutant *MUTYH* construct synthesis was accomplished using PCR-based site-directed mutagenesis of wild type *MUTYH*.

The wild type and mutants were then cloned as maltose binding protein (MBP) fusions into pMCSG19 (27) between the KpnI and XbaI restriction sites to increase protein solubility (28). The plasmids were further modified by removing the first fourteen codons encoding the mitochondrial recognition sequence, which alleviated heterologous protein toxicity. Furthermore, to decrease the capture of truncated heterologous protein, the N-terminus His₆ tag located between the MBP sequence and the TEV cleavage site was removed and a C-terminus His₁₀ tag was attached with a flexible (SG)₇ linker to increase solvent exposure.

Preparation of Protein

Heterologous MUTYH proteins in *Escherichia coli* strain BL21(DE3) were initially purified in accordance with previously published protocols using nickel affinity chromatography with 1 mM DTT (29). To improve yields and purity, the expression plasmids were transformed into the *E. coli* expression strain for toxic proteins, BL-AI (Invitrogen) also harboring the rare codon plasmid pRARE2-CDF (30). One liter of fresh Terrific Broth modified with 4% glycerol and 50 µg/mL of antibiotics (ampicillin and streptomycin) in a three L baffled flask was inoculated with 25 mL of overnight cultures in the same medium. Cultures were grown at 37 °C in a horizontal shaker at 175 rpm until the OD₆₀₀ reached approximately 2.5. The temperature was adjusted to 15 °C, and after 90 minutes, 0.25 mM IPTG and 0.2% arabinose were added. After 12-16 hours, cells were harvested by centrifugation, flash frozen in liquid nitrogen, and stored at -80 °C until processing. Cell pellets were thawed in an ice bath and re-suspended in 80 mL of ice cold 10% glycerol before the addition of 53 mg/mL of CelLytic Express (Sigma), one tablet of Protease Inhibitor Cocktail (Sigma) and 20 mM imidazole. The samples were clarified on a nutator for 30 minutes at 4°C before the addition of 20 mM of β-mercaptoethanol. The crude cell lysate was passed through a 0.45 µm filter in preparation for nickel affinity chromatography.

His-tagged proteins were loaded onto a 5 mL HisTrap HP column (GE Healthcare) at 2 mL/min using an AKTA Explorer FPLC instrument (GE Healthcare) at 4 °C. The columns were first washed with 20 column volumes of 93% Buffer A (20 mM Tris-HCl, pH 7.4, 1 M NaCl, 20 mM β -mercaptoethanol, 10% glycerol) and 7% Buffer B (20 mM Tris-HCl, pH 7.4, 100 mM NaCl, 500 mM imidazole, 10% glycerol) and the proteins were eluted using a 7-100% Buffer B gradient over 10 column volumes. Fractions containing MBP-MUTYH protein (as determined by SDS-PAGE), were pooled. Typical yields of purified protein for MBP-MUTYH wild type, Y179C and G396D were between 10-20 mg from one liter cultures and 0.5-1.5 mg of soluble protein was obtained for MUTYH p.C306W. Monomeric protein was obtained by size exclusion chromatography using a Superdex 200 10/300 GL column (GE Healthcare) in Buffer C (20 mM Tris-HCl, 100 mM NaCl, 1 mM DTT, 10% glycerol). Fractions eluting near the expected molecular weight (104 kD) were collected, partitioned into aliquots, flash frozen in liquid nitrogen, and stored at -80 °C until further use.

DNA Substrates for Glycosylase and Binding Assays

All oligonucleotides (Integrated DNA Technologies, Coralville, Iowa) were purchased PAGE purified. Duplexes were obtained by heating 50 μ l 50 μ M complementary strands at 85 °C then decreasing the temperature by 0.5 °C every 30 seconds until attaining room temperature. The FAM labelled 8-oxoG:A duplex used in the DNA glycosylase assay consisted of 5'-ACA AAG AAC TTA TAG CTC CTC CTT GAG CAC ACA GAG GTG TTC GAT GTA GTT G/A/C GCA GGA CGG GTT CAG T/6-FAM/-3' and 3'-TGT TTC TTG AAT ATC GAG GAG GAA CTC GTG TGT CTC CAC AAG CAT GAT CAA C/8oxoG/G CGT CCT GCC CAA GTC A-5'. The biotin labeled 8-oxoG:A duplex used in the binding assay consisted of 5'-

/BiotinTEG/AC AAA GAA CTT ATA GCT CCT CCT TGA GCA CAC AGA GGT GTT CAT
GTA GTT G/A/C GCA GGA CGG GTT CAG T-3' and the 8-oxoG oligomer.

DNA Glycosylase Assay

The DNA glycosylase assay was adapted as previously reported (29, 31-32). The activity was evaluated by providing 10 nM of DNA substrate containing a single 8-oxoG:A mismatch to wild type or mutant MBP-MUTYH proteins (0-1000 nM) at 37°C in a buffer (20 mM Tris-HCl, pH 8.0, 100 mM NaCl, 1 mM EDTA, 1 mM DTT, and 0.1 mg/mL BSA). Reactions were quenched after 1 hour with 80 mM NaOH followed by heating the samples to 90 °C for 4 minutes, cooled, and then diluted with three volumes of formamide spiked with GeneScan™ 500 LIZ™ Size Standard (Invitrogen). DNA fragmentation was determined employing capillary electrophoresis (U-M DNA Sequencing Core, ABI 3730 DNA Analyzer). Traces were analyzed using Peak Scanner™ Software (version 1.0, Applied Biosystems). The percent of excised DNA was calculated as the ratio of the 6-FAM peak area migrating at 44 oligonucleotides to the total peak area (at 44 and 66 oligonucleotides).

Multiple Turnover Assay: Active Site Titration

The multiple turnover assay was adapted as previously reported (29, 31-32). Reactions were analyzed for scission of 10 nM FAM-labeled 8-oxoG duplex DNA after the addition of MUTYH protein. The total protein concentrations, selected to give a burst amplitude in a detectible range, were 25, 2670, 500, and 25 nM of MUTYH wild type, Y179C, C306W, and G396D, respectively. Samples were drawn over a 20-minute time course and processed as described above. The cleaved product concentration, [P], was fitted with Equation 1 to determine the amplitude of the burst (A_0), k_B (rate constant during the burst phase) and k_L (rate constant for the linear phase).

Equation 1: $[P] = A_0[1 - \exp(-k_B t)] + k_L t$

The percent of active protein was calculated as a ratio of the A_0 to total protein concentration.

Binding Kinetics (Biolayer Interferometry)

All biolayer interferometry measurements were made on an Octet RED instrument (Pall ForteBio, Menlo Park, CA) using streptavidin (SA) biosensors (33). Assays were performed in 96-well black microplates at 25 °C and 1000 rpm. All volumes were 200 μ L. All proteins were buffer exchanged using PD-10 columns (GE Healthcare) pre-equilibrated with PBS then serially diluted (25, 12.5, 6.25, 3.125, 0.78125 nM) into working volumes with 1X Kinetics Buffer (Pall ForteBio; 10 mM Phosphate, pH 7.4, 150 mM NaCl, 0.02% Tween-20, 1 mg/mL BSA). The biotinylated duplex DNA was first immobilized onto the SA biosensors for 300 seconds and then equilibrated in 1X Kinetics Buffer for 300 seconds. Protein association was performed for 150-300 seconds followed by dissociation into 1X Kinetics Buffer for 900 seconds. A reference sensor with immobilized dsDNA was subtracted from each data set. Shift data was analyzed with ForteBio's Analysis software (version 7.1). Kinetic parameters k_{on} and k_{off} and affinity (K_D) were determined from a global non-linear regression of association and dissociation binding kinetics using a 1:1 Langmuir binding model.

Fe Elemental Analysis

The presence of elemental Fe within MUTYH protein samples was determined using a Thermo Scientific Element2 ICP-HRMS (34). Purified proteins were dialyzed overnight to remove glycerol and to allow equilibration with blank buffer (20 mM Tris-HCl, pH 7.5, 100 mM NaCl and 1 mM DTT) using a 10K MWCO Slide-A-Lyzer dialysis cassettes (Thermo Scientific).

DNA Synthesis and Purification for Electrochemistry

Thiol, FA, and OG modified DNA strands were prepared on an automated DNA synthesizer (Applied Biosystems) and purified by HPLC on a PLRPS column (Agilent) as described in previously published protocols (35); unmodified strands were ordered from IDT and purified by HPLC. For electrochemistry, 50 μ L 50 μ M complementary DNA strands were degassed and annealed in storage buffer (5 mM sodium phosphate, pH 7.0, 50 mM NaCl) in equimolar amounts by a 5-minute incubation at 95°C followed by slow cooling (1.5 hours) to RT on a thermocycler. Well-matched (WM) duplex DNA, DNA with an FA:OG lesion, and substrates containing an abasic site were all prepared in this way. Duplex sequences were as follows:

WM DNA

5' – ACT GAA CCC GTC CTG CGT CAA CTA CAT GAA CAC CTC – 3'
3' – TGA CTT GGG CAG GAC GCA GTT GAT GTA CTT GTG GAG – 5' – C6 Thiol

FA:OG DNA

5' – ACT GAA CCC GTC CTG **CGOG** CAA CTA CAT GAA CAC CTC – 3'
3' – TGA CTT GGG CAG GAC **GCFA** GTT GAT GTA CTT GTG GAG – 5' – C6 Thiol

Abasic DNA

5' – ACT GAA CCC GTC CTG CGT CAA CTA CAT GAA **CAbC** CTC – 3'
3' – TGA CTT GGG CAG GAC GCA GTT GAT GTA CTT GTG GAG – 5' – C6 Thiol

OG = 8-oxoguanine, FA = 2'-fluoroadenine, Ab = abasic site

Electrochemistry on DNA Self-Assembled Monolayers (SAMs)

Electrochemical characterization of MUTYH was carried out on a multiplexed chip platform consisting of 16 individually-addressable gold electrodes separable into four quadrants (35). Self-assembled DNA monolayers were formed by adding 25 μ L 25 μ M duplexed DNA in phosphate buffer (5 mM sodium phosphate, pH 7.0, 50 mM NaCl) to each quadrant of the chip

and incubating overnight. After monolayer formation, gaps in the film were eliminated by backfilling for 45 minutes at RT with 1 mM 6-mercapto-1-hexanol in phosphate buffer with 5% glycerol. The surface was then extensively rinsed in phosphate buffer, followed by protein storage buffer (described below). To compare different monolayer morphologies, DNA was incubated in phosphate buffer as described to generate low-density DNA monolayers (surface coverage of ~ 15 pmol/cm²) or in the presence of 100 mM MgCl₂ to form high-density monolayers (surface coverage of ~ 40 pmol/cm²) (36, 37). Bulk electrolysis experiments were performed using gold rod electrodes in a custom-made electrochemical cell. Experiments were carried out in air unless otherwise noted; anaerobic experiments were performed in a glove bag (Coy) under a 95% N₂/5% H₂ atmosphere.

MUTYH concentration was determined by UV-vis, using an extinction coefficient of 17000 M⁻¹cm⁻¹ at 410 nm to determine [4Fe4S] cluster concentration and 102330 M⁻¹cm⁻¹ at 280 nm to determine total protein concentration; cluster loading was determined by dividing [4Fe4S] cluster concentration by total protein concentration, and was typically around 15%. Initial characterization was carried out in Tris storage buffer (20 mM Tris, pH 7.4, 100 mM NaCl, 1 mM DTT, 10% glycerol v/v), while later electrochemical and spectroscopic experiments used a HEPES buffer (20 mM HEPES, pH 7.4, 100 mM KCl, 1 mM DTT, 0.5 mM EDTA, 10% glycerol v/v). MUTYH was transferred into HEPES using Amicon 10 kDa MW cutoff spin tubes (Millipore Biomedicals) at 4°C.

Once in an appropriate buffer, MUTYH was added to a multiplexed chip and incubated for several hours with cyclic and square wave voltammetry (CV and SQWV, respectively) scans taken once per hour. In typical experiments, CV scans were taken in a potential window of -0.188 to 0.412 V vs NHE at a scan rate of 100 mV/s, while SQWV scans were taken at a

frequency of 15 Hz with 0.025 V amplitude. To plot the scan rate dependence of CV current, scans in the same window were carried out at 20, 50, 80, 100, 200, 500, 750, and 1000 mV/s. All experiments were performed on a CH Instruments potentiostat with a Ag/AgCl reference in 3 M NaCl and Pt wire counter electrode. Potentials were converted to NHE by adding 212 mV to the measured potentials, accounting for both the salt concentration (209 mV according to BASi®) and ambient temperature (38). Bulk electrolysis was carried out at 0.412 mV versus NHE, and yields were estimated by subtracting the total charge passed with only buffer present from that passed when MUTYH was included. All buffer components were purchased from Sigma-Aldrich, the Ag/AgCl reference electrode was purchased from BASi®, and the Pt wire counter electrode was purchased from the Kurt J. Lesker Company.

EPR Spectroscopy

Continuous wave X-band EPR was carried out at 10 K on a Bruker EMX instrument. Samples were prepared aerobically, using 150 μ L 5 – 15 μ M MUTYH in parallel with a storage buffer blank. Spectra were taken from the summation of 9 sweeps at 12.88 mW microwave power, 2 G modulation amplitude, and a receiver gain of 5.02×10^3 .

Results

Identification and Functional Deficiencies of a Novel MUTYH Variant

A novel germline *MUTYH* variant, c.918C>G (p.C306W), together with the previously well-described *MUTYH* mutation, c.1187G>A (p.G396D), were identified in a patient with colonic polyposis and a family history significant for early age colon cancer. The cysteine at position 306 represents one of the four cysteine residues that mediate integration of the conserved MUTYH [4Fe4S] cluster. In bacterial MutY cluster loss is associated with decreased protein function (19) which suggests that in MUTYH the C306W variant may affect the integrity of the [4Fe4S] cluster and represent a pathologic mutant (Figure 4.1 illustrates the structure of bacterial MutY and identifies corresponding residues in MUTYH).

Supporting the potential pathogenicity of the novel c.918C>G variant, we established that this variant was situated in a trans chromosomal configuration relative to the c.1187G>A *MUTYH* mutation (Figure 4.2). Further evidence of the pathogenic nature of the c.918C>G variant was apparent in the sequencing of the *APC* gene in somatic DNA originating from a colonic adenoma from the patient. This sequencing revealed the presence of a C:G to T:A transversion in the *APC* gene, which is the hallmark genetic lesion distinguishing deficient *MUTYH*-mediated DNA repair (4) (Figure 4.3).

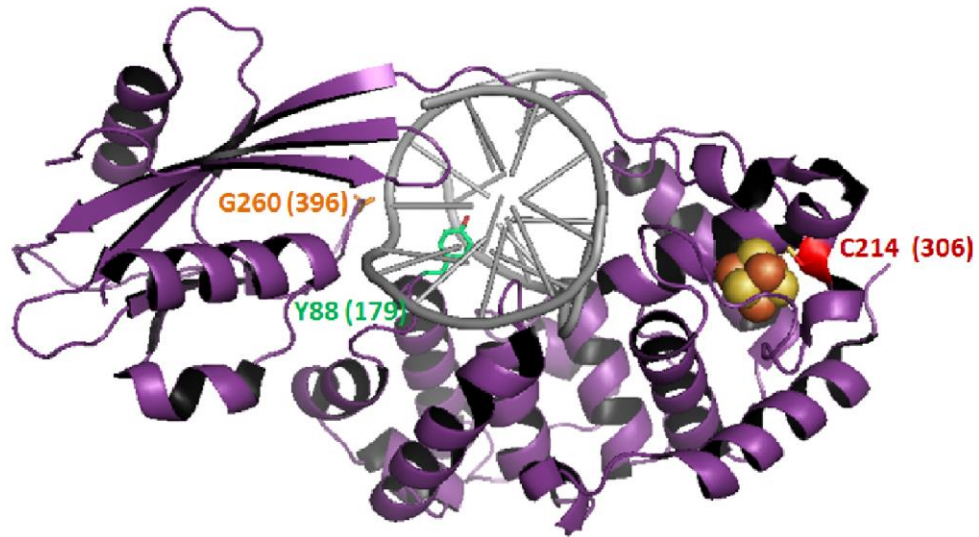


Figure 4.1 Structure of *Geobacillus stearothermophilus* MutY with residues homologous to disease-relevant variants in human MUTYH isoform $\beta 3$ highlighted. Y179C and G396D have been previously shown to be pathological mutations involved in MUTYH-associated polyposis (MAP); C306W was identified in this study. Notably, C306 is one of four cysteine residues involved in [4Fe4S] cluster ligation. Structure from PDB ID 1RRQ.

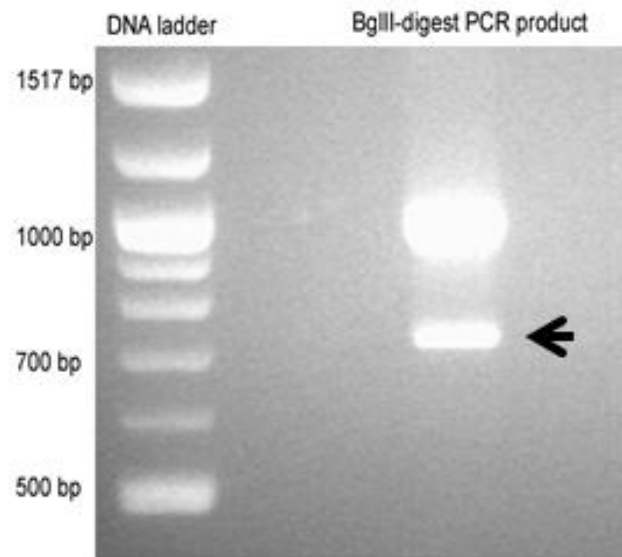


Figure 4.2 The c.918C>G *MUTYH* variant is situated trans relative to the c.1187G>A *MUTYH* mutation. The c.1187G>A (p.G396D) *MUTYH* mutation creates a unique *Bgl*III restriction enzyme site which we employed to isolate the chromosomal DNA strand containing the c.1187G>A *MUTYH* mutation. A 957 bp fragment encompassing the *MUTYH* open reading frame nucleotide positions 918 and 1187 was generated with PCR and then restriction enzyme digested with *Bgl*III. The digestion products were resolved on 1.5% agarose gel and the lower molecular weight DNA band isolated (arrow). Sequencing of the lower molecular weight band demonstrated the wildtype cytosine nucleotide at position 918 consistent with a trans configuration of the c.1187G>A and c.918C>G *MUTYH* alterations.

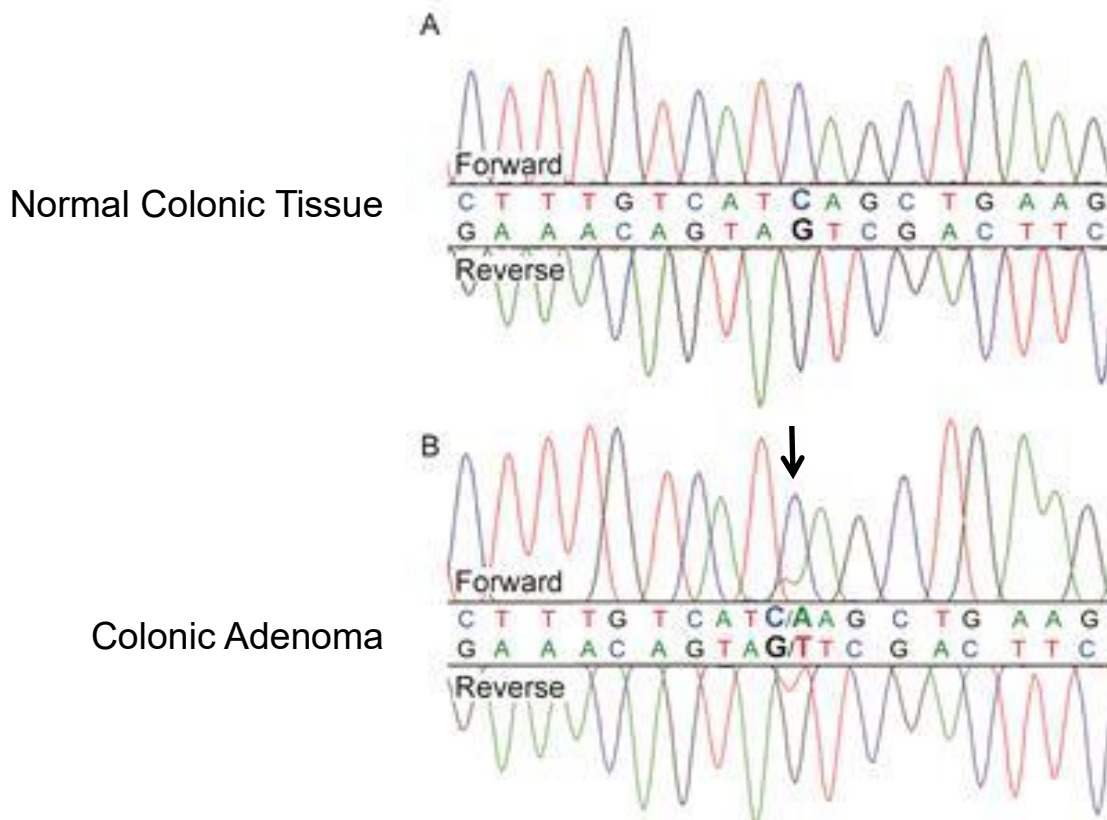


Figure 4.3 Trans c.1187G>A (p.G396D) and c.918C>G (p.C306W) MUTYH mutations are associated with the signature G:C to T:A transversion in the APC gene distinctive of deficient MUTYH DNA repair. From one of the patient's adenomatous polyps we extracted DNA to assess for the presence of the signature G:C to T:A nucleotide transversion which results from deficient MUTYH DNA repair. The figure depicts a portion of the germline nucleotide sequence from the mutation cluster region of the APC gene (upper tracing); this sequence reveals the normal wildtype APC sequence. In comparison, the lower tracing depicts the forward and reverse nucleotide sequence from DNA extracted from one of the patient's colonic polyps for this same mutation cluster region of the APC gene; there is identified a G:C to T:A transversion (arrow) resulting in a premature stop codon in the APC open reading frame and pathologic APC protein product.

Preparation of Monomeric MUTYH Protein

The four MUTYH proteins, WT, G396D, Y179C, and C306W were overexpressed in *E. coli* and purified by nickel affinity chromatography followed by size exclusion FPLC (Figure 4.4). All of the MUTYH proteins eluted as soluble aggregates in the void fraction; evidence of aggregation in these samples was also clear from the UV-visible spectra. Aggregated WT, G396D and Y179C MUTYH proteins demonstrated glycosylase activity consistent with previous reports, with attenuated activity observed in the G396D and Y179C MUTYH proteins (29-31); aggregated C306W protein lacked glycosylase activity (Figure 4.5a).

Aggregated protein is unlikely to exhibit native activity levels; thus, 20 mM β -mercaptoethanol was added prior to purification in an effort to disperse the aggregates and yield monomeric protein. This additional measure was effective, and monomeric proteins were of expected molecular weight (104kD) and eluted around 12 minutes during the size exclusion FPLC step (Figure 4.4). Relative to aggregated protein, monomeric WT demonstrated enhanced glycosylase activity. The glycosylase activities of the monomeric G396D and Y179C MUTYH proteins were also enhanced relative to the aggregated species, however they displayed less activity compared with WT protein. Monomeric C306W MUTYH protein remained severely deficient in glycosylase activity (Figure 4.5b). Based on the higher catalytic function of native, monomeric MUTYH protein was employed for all subsequent experiments.

For a more complete functional comparison of the four MUTYH variants, time course glycosylase assays were conducted under multiple turnover conditions to quantitatively determine the proportion of active enzyme in each sample (29, 31-32). These assays were performed using dsDNA containing an 8-oxoG:A mispair together with varying concentrations of MUTYH proteins. The experimental results demonstrate an initial burst of adenine excision activity proportional to the active fraction, A_0 , of the protein sample (Figure 4.5c, Table 4.1).

The rate constants, k_B and k_L , were determined for the exponential and linear phases of the reaction, respectively (Table 4.1). Both WT MUTYH and G396D proteins had comparable linear rates for turnover and the highest fraction of active protein. In contrast, the C306W MUTYH mutant was essentially devoid of adenine excision activity and Y179C had no detectable turnover. The fractions of active MUTYH were then employed to correct for the total amount of protein used in the glycosylase assay (Figure 4.5d), confirming that WT MUTYH and G396D mutant had comparable activities, while C306W and Y179C mutants displayed poor activity. Poor activity observed in MUTYH C306W could have two possible explanations: that either this mutant was catalytically inactive or it was unable to bind specifically to DNA (as is the case with low activity in the weakly-bound Y179C).

To help distinguish between these possibilities, we employed biolayer interferometry (BLI) (33) to measure the binding parameters of the MUTYH proteins. After preliminary experiments demonstrated that there was no significant difference in binding of WT MUTYH to DNA that contained an 8-oxoG:A mispair relative to DNA without the mispair, we compared the binding of WT MUTYH and the G396D, Y179C, and C306W mutants to DNA containing an 8-oxoG:A mispaired duplex. The binding kinetics data are summarized in Table 4.2. Relative to WT MUTYH, the G396D and Y179C variants demonstrated increasing values of K_D primarily due to decreased association rates. There was no detectable binding for the C306W mutant within the protein concentration range tested, suggesting that the low activity levels observed in this mutant were due primarily to ineffective DNA binding.

Together these data demonstrate the functional deficiency of the C306W MUTYH mutant. The cysteine at position 306 represents one of the four cysteine residues that ligate the MUTYH [4Fe4s] cluster. In bacterial MutY, [4Fe4S] cluster loss is associated with decreased

protein function (19), which suggests that the C306W variant of MUTYH may affect the integrity of the [4Fe4S] cluster accounting for this mutant's pathogenicity.

To assess the integrity of the [4Fe4S] cluster, iron loading of the clusters of WT MUTYH and the mutants Y179C, G396D and C306W were compared by quantifying the iron present in each sample using ICP-HRMS for elemental analysis (34). Consistent with disruption of the Fe-S cluster loop in the C306W variant, this protein exhibited substantially lower iron content relative to the other MUTYH proteins tested (Table 4.3). However, UV-visible spectra taken from disrupted aggregates of all four variants distinctly showed the broad peak centered at 410 nm that is characteristic of a [4Fe4S] cluster, indicating that MUTYH C306W is still capable of binding an intact cluster and further suggesting that loading by cellular machinery remains effective (Figure 4.6). In addition, circular dichroism (CD) spectra of WT MUTYH and the C306W mutant were indistinguishable, confirming that no global conformational changes were induced by the mutation (Figure 4.7). Thus, the low cluster content as measured by ICP-HRMS was instead tentatively associated with decreased protein stability in this mutant, and subsequent electrochemical and EPR experiments were used to more reliably examine the [4Fe4S] cluster properties in detail.

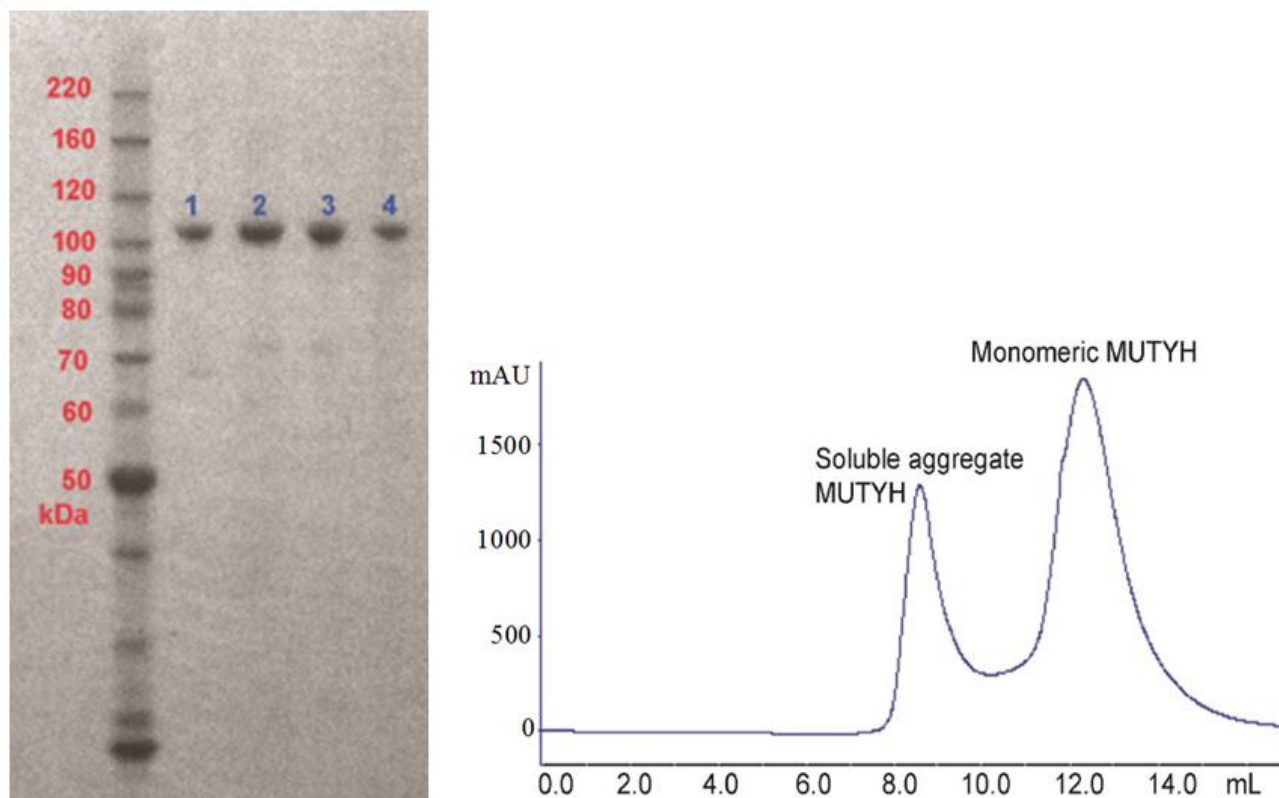


Figure 4.4 Purification of monomeric MUTYH proteins. **(Left)** SDS-PAGE gel of purified monomeric MUTYH proteins. The left lane contains the protein molecular weight ladder. The lanes 1-4 contain 1 μ g of MUTYH wild type, Y179C, C306W, and G396D, respectively. **(Right)** SEC-FPLC UV₂₆₀ trace of WT MUTYH following treatment with 20 mM β -mercaptoethanol. While some soluble aggregates still occur in the void volume, the majority of the purified protein is monomeric.

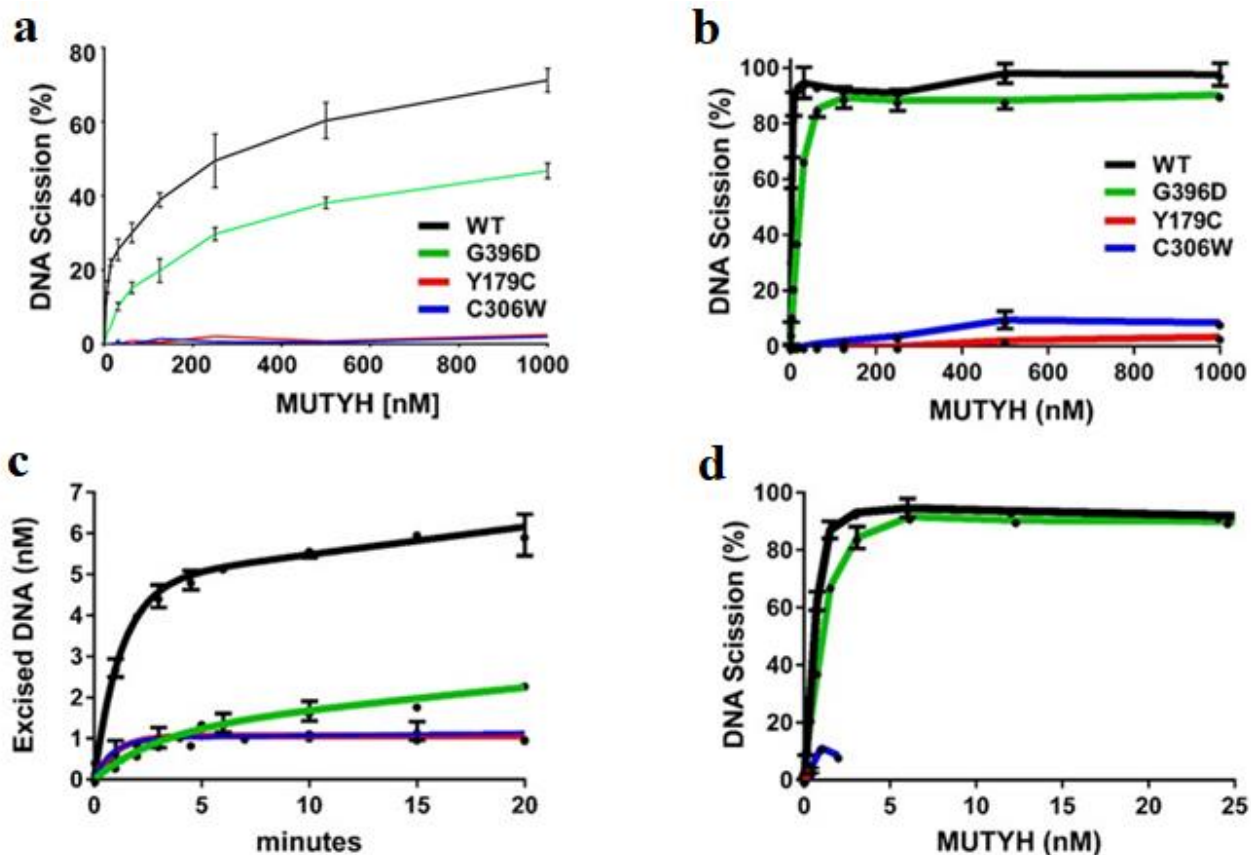


Figure 4.5 A novel human MUTYH variant, C306W, lacks glycosylase activity. Black lines, wild type MUTYH; Green lines, G396D; Red lines, Y179C; Blue lines, C306W

All data are presented as mean \pm s.d., $n = 3$.

(a) Glycosylase assays with soluble MUTYH aggregates. Activity levels for WT MUTYH and the variants Y179C and G396D are comparable to previously reported values. MUTYH C306W shows only minimal activity, comparable to Y179C.

(b) Glycosylase assay using soluble, monomeric MUTYH. The pattern matches that of aggregated protein, and confirms the observed defect in MUTYH C306W. Relative to WT and G396D MUTYH, Y179 and C306 proteins demonstrate severely attenuated DNA scission activity.

(c) Multiple turnover reaction conditions define the concentration of active protein within a purified protein sample. The glycosylase assay was performed with sufficient MUTYH protein to generate reaction burst amplitudes (A_0) within the detectable range. MUTYH active fractions, A_0 , and k_B and k_L rate constants of the excision reaction during the exponential and linear phase, respectively, were determined by fitting the curves from the reactions at top to the equation $[P] = A_0 [1 - \exp(-k_B t)] + k_L t$.

(d) Adenine excision activity of wild type and mutant MUTYH proteins after correcting for active fractions, A_0 . The correction for active MUTYH C306W and Y179C proteins shifted their assay concentrations below 2.5 nM.

Table 4.1 Determination of Rate Constants from Multiple Turnover Assay

Enzyme ID	[protein] (nM)	A₀	A₀/[protein]	k_B (min⁻¹)	k_L (min⁻¹ nM)
Wild type (WT)	25	4.8 ± 0.2	19.2%	0.8 ± 0.1	0.07 ± 0.01
Y179C	2670	1.1 ± 0.1	0.04%	1.0 ± 0.2	0
C306W	500	1.0 ± 0.1	0.2%	1.2 ± 0.2	0.01 ± 0.01
G396D	25	1.2 ± 0.2	4.9%	0.3 ± 0.1	0.05 ± 0.01

Data show mean ± s.d., $n = 3$

Table 4.2 Enzyme/DNA Kinetic Binding Data Obtained from Biolayer Interferometry.

Enzyme ID	k_{on} (1/Ms) x 10^4	k_{dis} (10^{-4} 1/s)	K_D (10^{-9} M)
WT	43 ± 0.4	2.7 ± 0.03	0.6 ± 0.01
Y179C	2.9 ± 0.4	5.0 ± 0.21	17 ± 2.57
C306W	No binding	-	-
G396D	10 ± 0.5	5.3 ± 0.12	5.2 ± 0.27

Data show mean \pm s.d., $n = 3$

Table 4.3 Elemental iron analysis of MUTYH proteins by ICP-HRMS.

Enzyme ID	[Fe] (μM)	[MUTYH] (μM)	% Ratio 4Fe/ Enzyme
WT	6.42 ± 0.32	1.36	115%
Y179C	6.40 ± 0.32	1.65	95%
C306W	0.78 ± 0.03	1.63	9%
G396D	6.59 ± 0.33	1.62	99%
Buffer	0.17 ± 0.03	-	-

Data show mean \pm s.d., $n = 3$

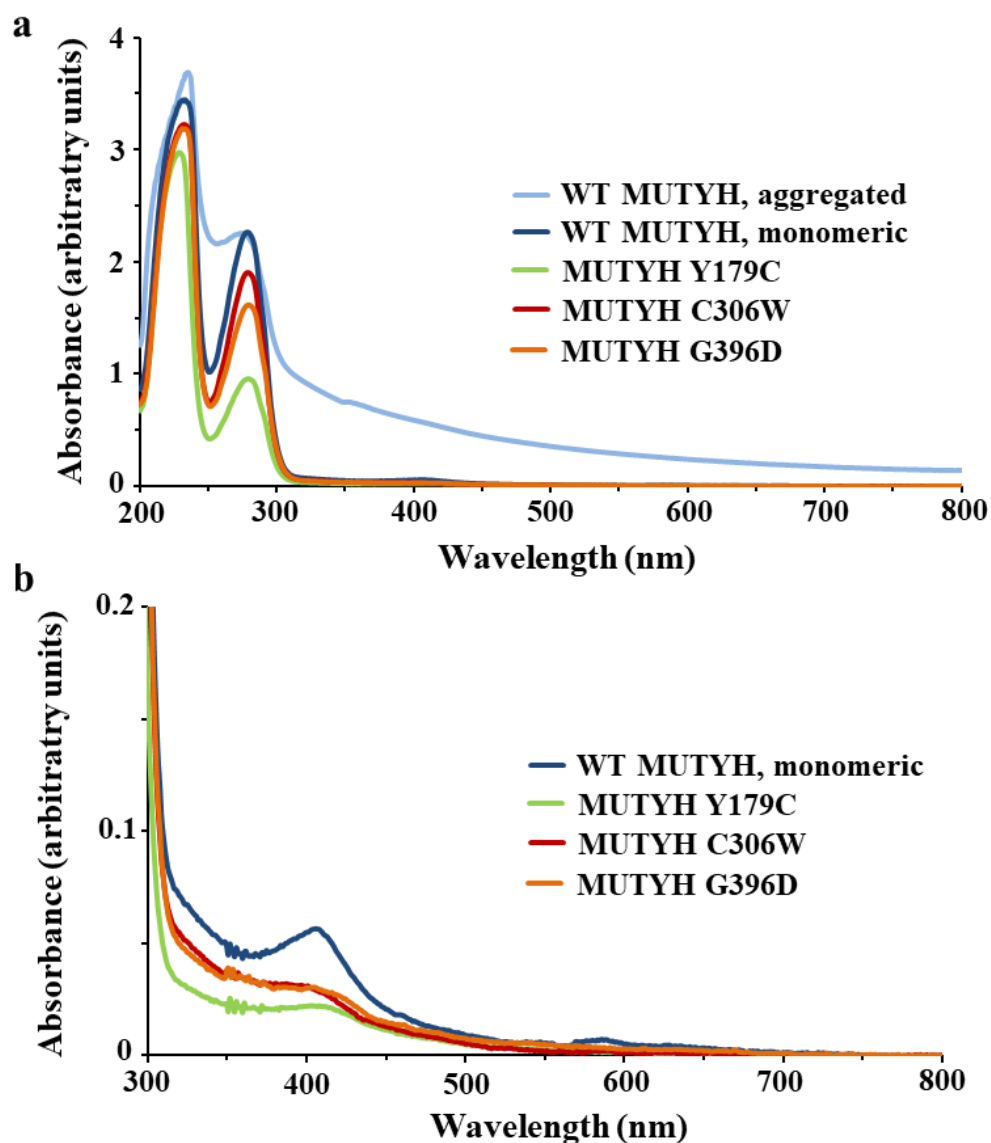


Figure 4.6 MUTYH UV-visible spectra. **(a)** Complete UV-visible absorption spectra of monomeric WT MUTYH and the mutants Y179C, C306W, and G396D. Aggregated MUTYH (light blue) can be distinguished by a U-shaped spectrum with elevated absorbance at 800 nm. **(b)** Zoomed in version of spectra in (a) highlighting the broad peak centered at 410 nm, which is characteristic of $[4Fe4S]^{2+}$ clusters. The presence of this peak confirms that the C306W mutation does not prevent cluster binding, and indeed cluster loading is comparable to that of WT and the other variants studied. All monomeric proteins were scanned in standard storage buffer (20 mM Tris-HCl, pH 7.4, 100 mM NaCl, 1mM DTT, 0.5 mM EDTA, 10% glycerol v/v), while the aggregated WT spectrum is in a phosphate buffer (20 mM sodium phosphate, pH 7.4, 100 mM NaCl, 0.5 mM EDTA, 10% glycerol v/v).

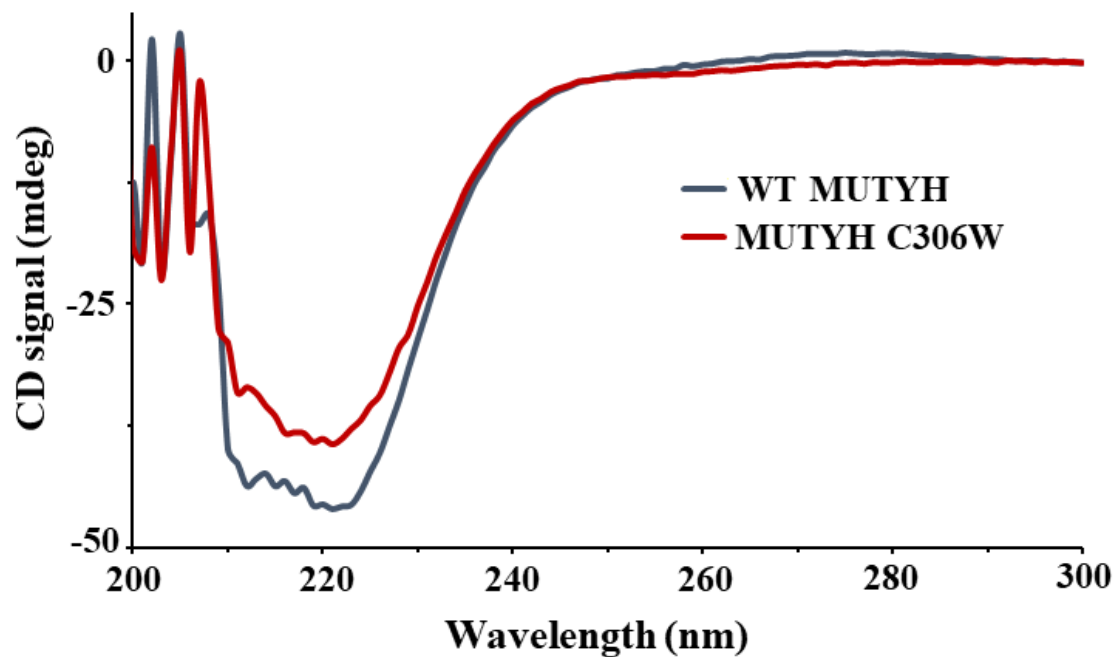


Figure 4.7 Circular dichroism (CD) spectra of WT MUTYH and MUTYH C306W. The similarity in spectra suggest that the C306W mutation does not result in significant global structural perturbations. These experiments were performed in HEPES storage buffer (30 mM HEPES, 100 mM KCl, 1 mM DTT, 0.5 mM EDTA, 10% glycerol v/v, pH 7.4).

DNA-Bound Electrochemistry of WT and Mutant MUTYH

Having observed that MUTYH C306W appeared to incorporate less iron despite its capacity to bind an intact cluster, we next assessed its redox properties on DNA-modified gold electrodes alongside WT, G396D, and Y179C MUTYH (Figure 4.8). Electrochemical analysis was reasoned to be an insightful approach in these studies for two reasons: first, access to highly purified WT MUTYH allowed us to determine if the human protein behaved like its bacterial counterpart, and, second, electrochemical monitoring would provide an effective way to assess the stability of MUTYH C306W over time. Specifically, the predicted instability of MUTYH C306W was expected to lead to electrochemical signals that were either smaller than WT or less stable over time.

In these experiments, MUTYH was incubated in storage buffer (20 mM Tris, pH 7.4, 100 mM NaCl, 1 mM DTT, 10% glycerol v/v) and periodically scanned by CV and SQWV. Aggregated protein preparations were treated with 20 mM β -mercaptoethanol and exchanged into storage buffer with fresh DTT immediately prior to electrochemical analysis. Cluster loading as determined by UV-visible spectroscopy was low in monomeric WT MUTYH prepared from disassembled aggregates (around 15% by the $A_{410}:A_{280}$ ratio), although all deaggregated MUTYH variants, including C306W, showed similar loading percentages. It is likely that apoproteins can compete to some extent with loaded holoenzyme for DNA binding on electrode surfaces, making low loading potentially problematic for electrochemistry. However, when making direct comparisons between different MUTYH variants, similar [4Fe4S] loading between the proteins studied is a more important factor than absolute loading as long as quantifiable signals can be obtained. Thus, we proceeded to electrochemical experiments despite the low loading values.

To test multiple conditions simultaneously, DNA monolayers were prepared on multiplexed gold electrodes, which enabled up to four experiments to be conducted in parallel (35). In this case, half of the available quadrants consisted of unmodified (WM) DNA and half of substrate trap FA:OG DNA included in an effort to enhance signal amplitude by increasing the DNA binding affinity. In addition, both high density (formed in the presence of 100 mM MgCl₂) and low density monolayers (formed without Mg²⁺) were compared on a single chip. DNA surface density is an important parameter for protein experiments (35): high density films have more DNA on the surface (30-50 pmol/cm²) that can improve DNA-mediated signaling by sterically hindering large proteins, while low density films contain less DNA (15-20 pmol/cm²) that can be more readily accessible to proteins (36, 37). Overall, the effect of each type of film is likely to depend strongly on the particular protein being studied, and both have been employed in previous studies.

In initial experiments, WT MUTYH (~2.5 μM [4Fe4S] cluster) yielded a reversible redox signal with a midpoint potential of 106 ± 1 mV versus NHE (Figure 4.8b), which is similar to the 65-95 mV (versus NHE) range reported for other DNA-bound [4Fe4S] proteins. That the MUTYH potential was slightly higher can most likely be attributed to disparate buffer conditions. The signal appeared almost immediately after addition to the electrode and increased in magnitude over the course of a 3-hour experiment. Although small, the signals were readily quantifiable: on low density films containing WM DNA, CV peak areas were $31 \pm 1 \times 10^{-2}$ nC for the reductive peak and $-33 \pm 2 \times 10^{-2}$ nC for the oxidative peak, while the equivalent values on high density films were $25 \pm 2 \times 10^{-2}$ nC and $-27 \pm 3 \times 10^{-2}$ nC, respectively. Interestingly, no significant differences in signal intensity were observed between WM and FA:OG DNA, with CV reductive and oxidative peak charges of $28 \pm 1 \times 10^{-2}$ nC and $-34 \pm 4 \times 10^{-2}$ nC on low

density FA:OG DNA films and $24 \pm 2 \times 10^{-2}$ nC and $-24 \pm 1 \times 10^{-2}$ nC on high density films. The FA:OG substrate trap is known to increase the binding affinity of the very similar murine MUTYH on a 30-mer duplex by an order of magnitude (39), and the absence of any clear change in signal intensity suggests that our system is not sufficiently sensitive to detect this difference. Several possible explanations exist for this insensitivity. First, it may be that the absolute amount of accessible DNA on either surface is too low to detect a difference between WM and FA:OG substrates. Alternatively, the significant amount of apoprotein present may have blocked some of the accessible DNA from fully loaded protein. Finally, the fact that DNA is tethered to a surface in these experiments rather than in solution might lower the chances of a successful binding event.

The potential and maximum signal size of MUTYH C306W ($\sim 2.5 \mu\text{M}$ [4Fe4S] cluster) were comparable to WT, although peak area was considerably more variable between experiments. Contrary to expectations, the C306W mutant was not obviously CT-deficient, but the signal did steadily decrease in size after 1-2 hours of incubation. The observed signal loss is consistent with the cluster lability suggested by ICP-HRMS. In addition, a second, irreversible peak centered around -50 mV versus NHE appeared and increased in size as the reversible [4Fe4S]^{3+/2+} signal decayed (Figure 4.8b). This pattern of reversible signal loss and secondary peak growth was observed in several experiments with C306W and did not occur to any appreciable extent in WT MUTYH, confirming that it was not a contaminant. A secondary peak at this potential was unprecedented among previously studied base excision repair proteins, but its growth along with the parallel loss of the reversible signal suggested that it was some form of degradation product.

While the DNA processing enzymes studied thus far have generally shown stabilization of the $[4\text{Fe}4\text{S}]^{3+}$ form upon DNA binding to yield a reversible $[4\text{Fe}4\text{S}]^{3+/2+}$ signal on an electrode, loss of iron by the oxidized $[4\text{Fe}4\text{S}]^{3+}$ species to form the $[3\text{Fe}4\text{S}]^+$ cluster has been reported in bacterial MutY and EndoIII when the samples were frozen for EPR under aerobic conditions (20). As the loss of one iron atom is the first step in cluster degradation, we considered the $[3\text{Fe}4\text{S}]^+$ cluster to be a likely candidate for the identity of the unexpected redox-active MUTYH C306W species. At ~ -50 mV versus NHE, the MUTYH C306W secondary peak fell within the range of reported $[3\text{Fe}4\text{S}]^+$ cluster potentials (40), supporting this assignment. The irreversible nature of the signal was unusual, given that $[3\text{Fe}4\text{S}]$ clusters can access a reversible $1^+/0$ redox couple, but, given the significant impact of even a single unit of cluster charge on DNA binding affinity (21), irreversibility in our experiments can be rationalized as protein dissociation from DNA following reduction to the neutral $[3\text{Fe}4\text{S}]^0$ state.

Confirming that the $[4\text{Fe}4\text{S}]$ cluster degradation observed in MUTYH C306W was unique to this mutant, electrochemical analysis of DNA bound Y179C and G396D (both $2.5 \mu\text{M}$ $[4\text{Fe}4\text{S}]$ cluster) yielded reversible signals at nearly the same potential as WT with no secondary peak present (Figure 4.8b, Table 4.4). Like WT, the signals from both of these variants increased over time and remained stable for several hours. Notably, the Y179C signal was only about half as large as WT, consistent with the lower DNA binding affinity of this mutant relative to both WT and G396D (K_D of 7.5 nM for Y179C versus 2.2 and 4.9 nM for WT and G396D, respectively) (29). Overall, both mutants were more similar to WT than C306W in their redox properties, an unsurprising outcome given that the cluster in these variants is unaltered. The propensity for the MUTYH C306W cluster to degrade by redox activity provides a possible explanation for the low DNA binding affinity observed with BLI binding studies, as previous

work with *E. coli* MutY has demonstrated that apoprotein lacking cluster is defective in DNA binding despite remaining structurally intact (19).

Characterization of the C306W Degradation Product

In an effort to characterize the MUTYH C306W cluster degradation product more fully, we proceeded to assess its dependence on oxygen, which is often an important factor in $[3\text{Fe}_4\text{S}]^+$ cluster formation (20). Specifically, electrochemical and UV-visible spectroscopic analysis were employed to compare aerobically oxidized proteins with those maintained in an anaerobic environment. For an effective comparison, a single C306W sample was concentrated and one half was diluted to 2.5 μM (by $[4\text{Fe}_4\text{S}]$ cluster) in degassed buffer and placed on a chip containing low density WM DNA in an anaerobic glove bag (95% N_2 /5% H_2 atmosphere), while the other half was maintained in aerobic conditions and oxidized on a DNA-modified gold rod electrode held at 0.412 V versus NHE. The anaerobic sample was scanned periodically by CV and SQWV, and, following electrolysis, the oxidized sample was transferred to the glove bag and added to a separate quadrant on the same chip. In addition to electrochemistry, UV-visible spectra were recorded before and after electrolysis both to observe changes in the 410 nm peak and to ensure that the oxidized sample did not aggregate.

Quantification of the total charge passed during electrolysis indicated near-complete oxidation of the aerobic protein by ~60 minutes. Prior to electrolysis, the UV-visible spectrum showed the broad peak centered at 410 nm characteristic of a $[4\text{Fe}_4\text{S}]$ cluster, but after oxidation, the absorbance increased over a broad range from 700 – 300 nm, with a poorly-defined peak around 410 nm and a substantial shoulder between 400 and 300 nm (Figure 4.8c). Such absorbance features are a general characteristic of cluster oxidation, although UV-vis spectra

alone are insufficient to precisely identify the oxidized species generated (41). Importantly, the 280 nm peak remained sharp and distinct even after oxidation, and the spectrum was not elevated at 800 nm, demonstrating that the protein had not aggregated and confirming that all changes were due solely to cluster oxidation. This result stands in stark contrast to the soluble MUTYH aggregates observed in both WT and C306W in the absence of DTT, which were visibly cloudy with a U-shaped UV-visible spectrum characteristic of aggregation, with highly elevated absorbance at 800 nm, no distinct [4Fe4S] peak, and a very slight 280 nm peak visible only as a shoulder.

CV and SQWV of the aerobically oxidized C306W MUTYH variant revealed an irreversible peak comparable in size to the main reversible peaks; in contrast, the equivalent peak in the anaerobic sample was much smaller than the main peak and had not changed from initial levels (Figure 4.8d). Furthermore, the reversible signal of the anaerobic sample increased over time and exceeded even the strongest signals observed for aerobically incubated WT MUTYH, which was all the more intriguing given that the anaerobic sample had been incubating on the electrode for several hours. Supporting greater instability of the C306W [4Fe4S] cluster, aerobic oxidation of WT MUTYH gave low bulk electrolysis yields, and no readily apparent irreversible peak was present by CV. In addition, the UV-vis spectra of WT before and after oxidation were indistinguishable. Taken together, the apparent sensitivity of MUTYH C306W to oxidation and degradation in air along with the absence of any observable degradation in aerobically oxidized WT MUTYH all supported the assignment of the secondary peak to a [3Fe4S]⁺ cluster. However, UV-visible spectroscopy and electrochemistry alone are insufficient to distinguish between possible oxidized Fe-S species, which requires EPR spectroscopy.

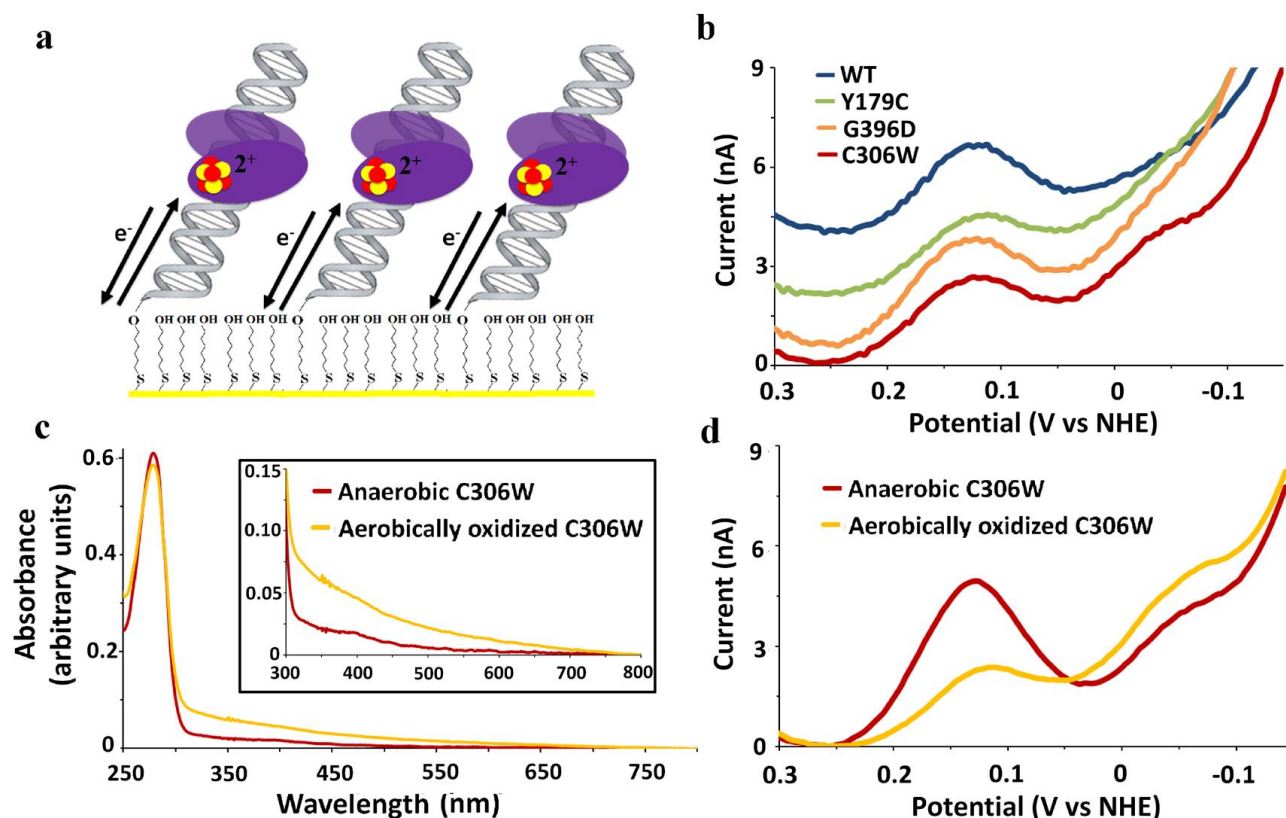


Figure 4.8 Initial electrochemical and spectroscopic characterization of MUTYH variants. (a) Electrochemistry is carried out on DNA-modified gold electrodes, which allow controlled reduction or oxidation of the [4Fe4S] cluster. (b) Incubation of 2-2.5 μM WT, Y179C, G396D, or C306W MUTYH on a DNA-modified electrode in storage buffer (20 mM Tris, 100 mM NaCl, 1 mM DTT, 0.5 mM EDTA, 10% glycerol v/v, pH 7.4) results in a reversible signal with a midpoint potential of approximately 105 mV versus NHE. C306W uniquely exhibited an irreversible reductive peak around -50 mV versus NHE, which was presumed to be some form of oxidative degradation product. (c) After aerobic oxidation by bulk electrolysis, the UV-vis spectrum of C306W showed no evidence of aggregation but did display a broad increase in absorption from 700 to 300 nm, suggestive of cluster oxidation. (d) Consistent with cluster degradation in the presence of oxygen, aerobic bulk electrolysis of C306W enhanced the size of the peak relative to the reversible signal, while anaerobic incubation provided a protective effect. All SQWV measurements were obtained at a frequency of 15 Hz and 0.025 V amplitude, and the signals shown are an average from at least four separate electrodes on a multiplexed chip. The SQWV background current levels in (b) were all comparable and have been adjusted for ease of visualization. Bulk electrolysis was performed for 1 hour at 0.412 V vs NHE on a DNA-modified gold rod electrode in a glass cell.

EPR Spectroscopy of MUTYH

Having confirmed that the secondary C306W reductive peak was an oxidation product formed under aerobic conditions, we turned to EPR spectroscopy as a final step toward its identification. EPR provides a means of distinguishing among different paramagnetic species and is commonly employed to study iron-sulfur proteins (40 - 42). While EPR analysis can be very informative, there were two general concerns with respect to MUTYH. First, EPR experiments are generally performed with significantly higher levels of concentrated protein than those used in our electrochemical experiments with MUTYH: signals have been reported for 10 μM *E. coli* EndoIII (20) and ~ 9 μM DNA polymerase δ (43), but even these were still 3-4 times more concentrated than the MUTYH samples. Second, the low temperatures necessary to resolve signals from [4Fe4S] clusters (10-35 K) require the samples to be frozen prior to analysis, which can impact protein stability if the buffer pH changes with temperature, as is the case for the Tris buffers employed in our MUTYH studies (44).

Therefore, prior to attempting EPR, all MUTYH variants were concentrated and exchanged into a HEPES buffer (20 mM HEPES, pH 7.4, 100 mM KCl, 1 mM DTT, 10% glycerol v/v, pH 7.4); potassium was used in place of sodium as a further precaution to stabilize the pH at low temperature (45). UV-visible spectroscopy and electrochemistry (Figure 4.9a, 10) were used to confirm protein stability in HEPES and to verify that redox properties remained comparable. As observed in the UV-vis spectra (Figure 4.9a), all of the MUTYH variants maintained their monomeric form in this buffer, although they could not be concentrated beyond 15 μM without forming soluble aggregates. When such aggregates did form, they were readily resolved by simple dilution, and the UV-visible spectra of WT MUTYH and the mutants Y179C and G396D all retained a sharp 410 nm peak with $\sim 15\%$ cluster loading even after an additional

freeze-thaw cycle one week after buffer exchange (Figure 4.9a). In contrast, the spectrum of the MUTYH C306W protein closely resembled the aerobically oxidized sample described previously (Figure 4.9a). Oxidation may have occurred over the extended aerobic buffer exchange process or during the freeze-thaw cycle on the day of EPR experiments. Because the extinction coefficient at 410 nm was unknown for the MUTYH C306W product, cluster loading in this mutant was estimated by comparing the magnitude of absorbance with the earlier aerobically oxidized sample, yielding a concentration comparable to the other variants.

All EPR spectra of MUTYH proteins were obtained with 15 μ M WT and C306W and 5 μ M G396D and Y179C (the latter mutants were not available in such large amounts). From the broadened UV-vis absorption, we predicted that the corresponding EPR spectrum would show evidence of either the $[3\text{Fe}4\text{S}]^+$ cluster or a more advanced degradation product, while WT, Y179C, and G396D were expected to be diamagnetic and thus EPR silent. Unexpectedly, all of the samples showed a small, broad signal with a shoulder at $g = 2.04$ (Figure 4.9b) most likely attributable to oxidation during the aerobic freezing process, as reported previously for *E. coli* EndoIII and MutY²⁰. Nonetheless, MUTYH C306W protein displayed a much sharper signal with a clear peak centered at $g = 2.018$ (Figure 4.9b), which is characteristic of $[3\text{Fe}4\text{S}]^+$ clusters (40, 42). Importantly, the C306W EPR signal, but not the broad signals of WT and the other MUTYH variants, closely resembled spectra from chemically oxidized *E. coli* EndoIII and MutY that were also assigned to the $[3\text{Fe}4\text{S}]^+$ cluster (20). While some of the C306W $[4\text{Fe}4\text{S}]$ degradation may have occurred during sample freezing, the significantly larger and sharper EPR signal relative to the other variants and the UV-visible spectrum indicating previous oxidation suggest that the cluster was largely in this state prior to freezing.

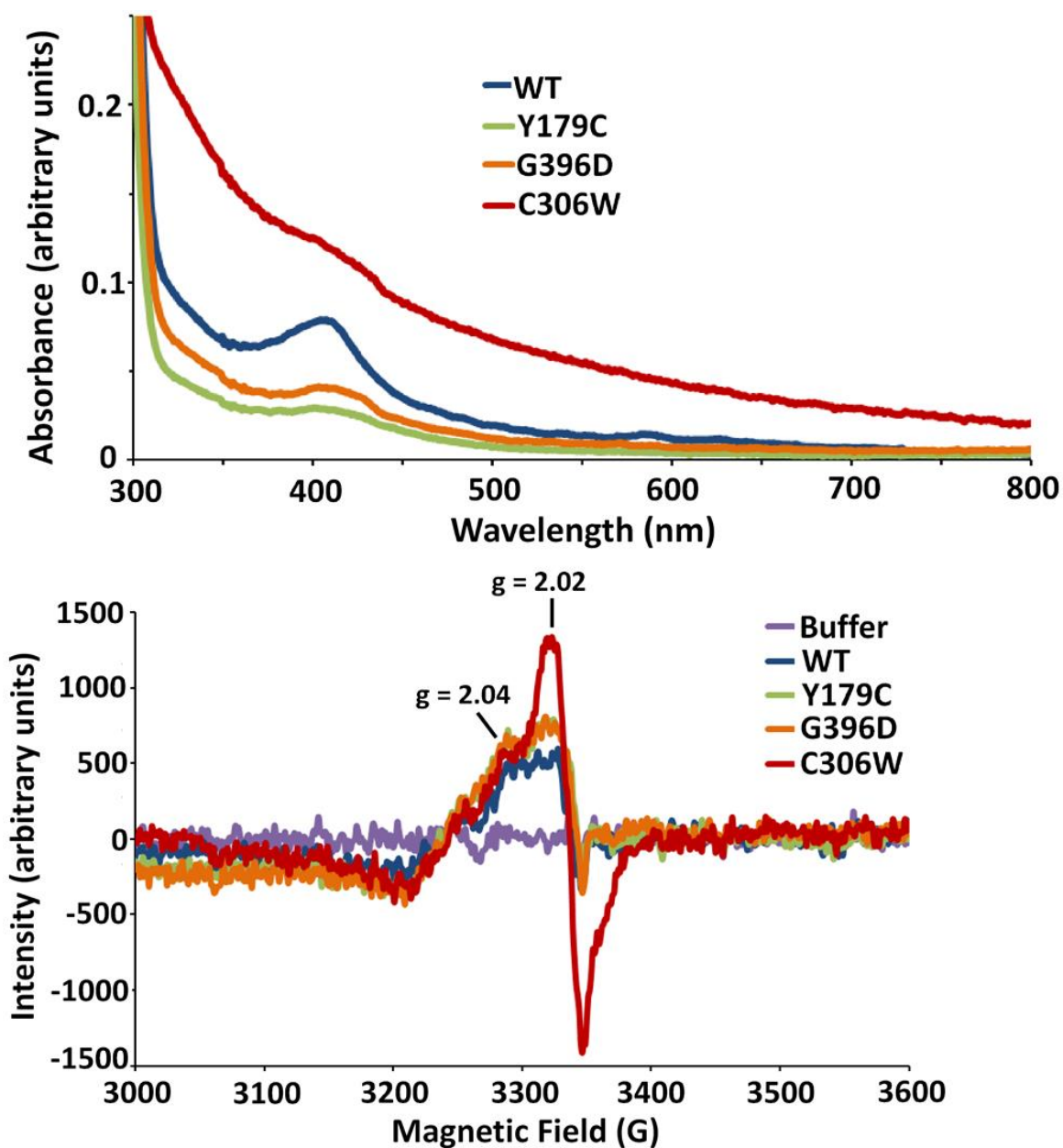


Figure 4.9 Characterization of MUTYH in HEPES and analysis of the C306W decay product. **(top)** UV-visible spectra of concentrated WT, Y179C, and G396D exchanged into HEPES buffer (30 mM HEPES, 100 mM KCl, 1 mM DTT, 0.5 mM EDTA, 10% glycerol v/v, pH 7.4) all displayed the characteristic [4Fe4S] cluster absorption band centered at 410 nm. In contrast, the C306W spectrum showed broadly increased absorbance associated with oxidation. **(bottom)** EPR spectra of 15 μM (WT and C306W) or 5 μM (Y179C and G396D) MUTYH variants. The C306W EPR spectrum shows a sharp peak at $g = 2.018$ with a shoulder at $g = 2.04$ EPR, supporting identification of the degradation product as a [3Fe4S]⁺ cluster. Continuous wave X-band EPR spectra were measured at 10 K with 12.85 mW microwave power, 2 G modulation amplitude, and 5.02×10^3 receiver gain.

Electrochemical Characterization of MUTYH in EPR Buffer

In parallel with EPR experiments, we performed electrochemistry with concentrated (5 μM) MUTYH in HEPES buffer to verify that the redox properties were comparable to those observed in Tris buffer (Figure 4.10). In HEPES buffer, the midpoint potential of WT MUTYH decreased from 105 ± 1 mV vs NHE in Tris to 93 ± 1 mV vs NHE (Table 4.4), but the overall signal shape and properties remained unaltered. Unsurprisingly, the addition of more concentrated protein to the electrode (~ 5 μM for all electrochemical experiments in HEPES) gave substantially larger signals, with WT MUTYH yielding a reductive peak area of 7.6 ± 3 nC and an oxidative peak area of -5.6 ± 3 nC on low density monolayers. Remarkably, although the protein was only about twice as concentrated compared with previous experiments, the signal was over 10 times larger, suggesting more efficient redox coupling in HEPES.

Like WT, all of the mutants showed ~ 10 -fold larger signals when concentrated in HEPES, and their midpoint potentials decreased by a similar margin, placing all variants in the same potential window (Table 4.4). The signal from the MUTYH Y179C protein was still noticeably smaller than WT (reductive and oxidative peaks at $48 \pm 18\%$ and $33 \pm 17\%$ of WT), most likely as a result of lower DNA binding affinity, while G396D was not significantly different from WT (reductive and oxidative peaks at $77 \pm 32\%$ and $76 \pm 41\%$ of WT). To ensure accurate comparison with EPR spectra, electrochemistry for the less stable C306W mutant was performed on the same day as EPR, and using the same sample stock. Consistent with the oxidation indicated in the UV-visible spectrum and the presence of a characteristic $[\text{3Fe4S}]^+$ cluster EPR signal, the electrochemical signal from this sample was significantly smaller than any other mutant (reductive and oxidative peaks $35 \pm 15\%$ and $26 \pm 14\%$ of WT) and possessed a prominent secondary reductive peak centered at -88 ± 6 mV vs NHE (Figure 4.10). The larger

signals made this peak much more readily quantifiable compared with Tris buffer, and the total charge of this irreversible peak was found to represent ~20% of either peak of the reversible $[4\text{Fe4S}]^{3+/2+}$ couple. The area in this case was lower than estimated for the C306W sample aerobically oxidized in Tris buffer, where the secondary peak was roughly equal in magnitude to the main peak, which suggested that the concentrated sample in HEPES was not 100% oxidized. Overall, UV-visible and EPR spectra obtained from the same MUYH C306W protein strongly supported the identification of the irreversible peak as a $[3\text{Fe4S}]^{+/0}$ redox couple. When compared to WT MUTYH, or even the Y179C and G396D mutants, the susceptibility of the C306W $[4\text{Fe4S}]$ cluster to degradation upon oxidation during redox signaling was apparent, and the irreversibility of the degradation product signal indicates that the resultant $[3\text{Fe4S}]^{+/0}$ species does not bind DNA effectively.

Based on the measured midpoint potentials in Tris buffer (Table 4.4), electrochemical signals from dilute MUTYH samples were most likely DNA-bound (35); however, the small signal sizes made it impossible to determine if the signal was DNA-mediated. The substantially larger signals recorded in HEPES buffer with concentrated samples allowed this issue to be addressed, and chips containing half well-matched DNA and half DNA containing an abasic site were prepared for this purpose. Earlier work with DNA-mediated EndoIII signals showed a dependence on monolayer morphology (35); thus, to see if this was also the case for MUTYH, the abasic site discrimination studies were carried out on both high and low density monolayers.

On abasic DNA, a maximum charge attenuation of 38% for the reductive peak and 46% for the oxidative peak was obtained on low density monolayers (Figure 4.11); in contrast, no appreciable discrimination was observed on high density monolayers. The observed abasic site discrimination confirmed that MUTYH can take part in DNA-mediated signaling, and the

differences in high and low density DNA monolayers emphasize the importance of surface accessibility to large proteins. The sterically hindered high density films clearly do not provide sufficient access to DNA in an appropriate conformation to observe such a signal, and the peaks seen in this case are likely attributable to DNA-bound proteins signaling directly through the monolayer surface (35).

Interestingly, the pattern of abasic site discrimination observed here is opposite to previously published data for *E. coli* EndoIII (35); this difference can be rationalized by considering two important factors. First, the DNA used in the EndoIII experiments was only 15 bp, while EndoIII has a binding footprint of 12 bp (46). Thus, the protein would have taken up much of the available space and the cluster could readily bypass the mismatch on fully accessible low density DNA. In contrast, the DNA substrate chosen for MUTYH was 36 bp while the binding footprint is likely close to the 16 bp reported for mouse MUTYH (39), making bypass of the abasic site on low density monolayers less likely. Second, a considerable size discrepancy exists between the two proteins: unmodified MUTYH is 61 kDa, while EndoIII is only 24 kDa. Thus, steric hindrance in high density films would be expected to have a greater impact on MUTYH, a notion supported by the observation that the largest signals obtained on high density monolayers containing WM DNA were ~30% smaller than the equivalent signals on low density films.

Table 4.4 CV Midpoint Potentials of MUTYH Variants in Tris and HEPES Buffers.

MUTYH variant	E_{mdpt} in Tris (mV)	E_{mdpt} in HEPES (mV)
WT	106 ± 1	93 ± 1
C306W	114 ± 3	97 ± 1
Y179C	105 ± 0.8	100 ± 2
G396D	115 ± 0.1	99 ± 4

Error is the standard deviation of the mean from at least 3 separate experiments.

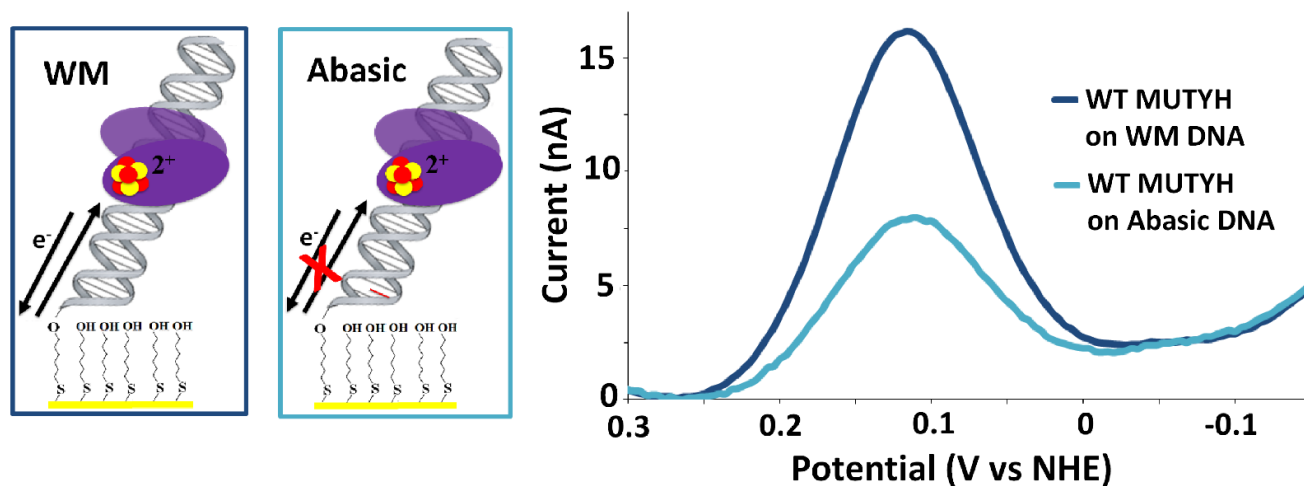


Figure 4.11 Abasic site discrimination by WT MUTYH. 5.0 μM WT MUTYH was incubated in HEPES buffer (30 mM HEPES, 100 mM KCl, 1 mM DTT, 0.5 mM EDTA, 10% glycerol v/v, pH 7.4) on a single multiplexed chip with half of the available quadrants containing DNA with an abasic site (light blue) near the electrode and the other half containing well matched (WM) DNA (dark blue). As is apparent from the SQWV voltammetry, the signal on WM DNA was comparable in size to previously observed signals (Figure 4.10), but the total peak area on abasic DNA was decreased by $\sim 40\%$, indicating that the signal was DNA-mediated. The SQWV voltammograms were obtained at 15 Hz and 0.025 mV amplitude, and signal shown is the average of at least seven separate electrodes on a single multiplexed chip.

Discussion

In the present study we describe a novel MUTYH variant, C306W, and its association with the development of colonic polyposis and a family history of colon cancer. We determined that the C306W variant lacks DNA abscission activity and has decreased ability to bind target DNA, establishing the pathogenicity of this variant. In C306W MUTYH there occurs loss of a cysteine residue that ligates the MUTYH Fe-S cluster. This finding raised the possibility that the loss of the cysteine might disrupt the integrity of the Fe-S cluster and be causative of the pathogenicity associated MUTYH C306W. The observation by ICP-HRMS that the Fe-S cluster of C306W exhibits significantly lower iron content provided further bolsters this hypothesis and prompted an electrochemical mechanistic investigation of the MUTYH Fe-S cluster and the effect of cysteine loss in the C306W variant.

Toward this end, in our investigation, we present the first direct evidence of redox signaling in eukaryotic MUTYH, which until now had only been assumed based on studies using *E. coli* MutY. DNA-modified electrochemical analysis revealed the redox potentials of all MUTYH variants studied to be in general agreement with earlier work (Table 4.4). Notably, the potentials as measured in HEPES buffer are almost identical to those obtained for *E. coli* MutY in phosphate buffer (20). The similarity of the WT MUTYH electrochemical signals to those of the *E. coli* protein strongly supports the notion that the primary function of the conserved Fe-S cluster is redox activity in all organisms. Furthermore, the DNA-mediated nature of this signal in MUTYH suggests that a process akin to the DNA-mediated redox-based damage search observed in bacteria may also be present and operating in humans.

Unlike WT MUTYH, the C306W mutant showed an unexpected, and irreversible, reduction between -50 and -100 mV versus NHE in combination with loss of the reversible

signal; EPR spectroscopy confirmed this additional signal to be the $[3\text{Fe4S}]^{+0}$ couple. The observed degradation and poor DNA binding in MUTYH C306W are consistent with the higher DNA binding affinity associated with increasing charge in $[4\text{Fe4S}]$ clusters, in which Coulombic effects cause the $[4\text{Fe4S}]^{3+}$ cluster to bind the DNA polyanion significantly more tightly than the $[4\text{Fe4S}]^{2+}$ form (21). The relationship of cluster charge to binding affinity predicts that the $[3\text{Fe4S}]^+$ and $[3\text{Fe4S}]^0$ degradation products, with one and zero net charges, would bind much more weakly to DNA than the $[4\text{Fe4S}]^{2+}$ form, and the irreversible reduction observed in degraded MUTYH C306W was experimentally verified. Overall, our results suggest that, for MUTYH C306W, ordinary redox activity on DNA would lead to oxidation to the $[4\text{Fe4S}]^{3+}$ state, as is typical in these proteins, but the lower stability of the cluster would promote the loss of an iron atom and irreversible dissociation following a second redox signaling cycle. Ultimately, this process could result in the low iron content measured by ICP-HRMS, an effect that might well be exacerbated if the dissociated $[3\text{Fe4S}]^0$ form degraded further when removed from the protective environment of DNA. Cluster degradation in MUTYH C306W is also consistent with the low levels of glycosylase activity and poor DNA binding affinity as measured by BLI (Table 4.2), which are attributes of bacterial MutY following cluster removal (19). This inherent instability of the C306W Fe-S cluster and consequent loss of function, we propose to be causative of pathogenicity this MUTYH variant.

With regard to other potential causes of pathogenicity, we recognize that MUTYH is also regulated by post-translational modifications, including phosphorylation and ubiquitination, that could be altered by this mutation (47, 48). However, these sites are in different regions of the protein relative the $[4\text{Fe4S}]$ domain, and are thus unlikely to be affected by this particular

mutation. Thus, redox-stimulated cluster degradation is most likely the primary cause of pathogenicity in MUTYH C306W.

The irreversible [3Fe4S] cluster signal seen in MUTYH C306W has not been previously observed in electrochemical studies of DNA-processing [4Fe4S] proteins, but the signal was within the same redox potential range reported for the [3Fe4S]⁺⁰ couple of bacterial nickel-iron hydrogenase and fumarate reductase enzymes (49-51). In *E. coli* MutY, [4Fe4S] cluster ligand substitution of the corresponding cysteine residue has been shown to result in defective DNA binding, similar to the situation with MUTYH C306W (52). It should be noted, however, that none of the substitutions involving *E. coli* MutY were to a residue as bulky or destabilizing as tryptophan (52).

Given the results obtained for MUTYH C306W, it appears probable that mutations in other residues that alter the region around the [4Fe4S] cluster will be similarly deficient in their ability to mediate repair of oxidatively damaged DNA *in vivo* (53-57). Indeed, four arginines participate in H-bonding to the four cysteines that coordinate with the [4Fe4S] cluster (56) (Table 4.5) and mutations to each one are associated with colorectal cancer (1). It is probable that these mutations also result in instability, degradation and dysfunction of the Fe-S cluster secondary to the same mechanisms detailed above. The effects of these lesions as well as the C306W variant underscore the importance of the [4Fe-4S] co-factor in establishing competent MUTYH-mediated DNA repair.

The current study advances our basic electrochemical understanding of the redox chemistry, function, and integrity of the [4Fe4S] cluster. Concomitantly, we are acquiring a better appreciation for the pathologic sequelae resulting from disruption of the Fe-S cluster. Specifically, within the context of the present investigation we have documented and provided

explanation for a novel mechanism of colonic polyposis and cancer predisposition caused by electrochemical compromise of the MUTYH [4Fe4S] cluster. Future studies, we anticipate, will provide further clarification of the central role of the cluster in MUTYH-mediated DNA repair and its underlying electrochemistry.

Table 4.5 The four coordinating cysteines and surrounding arginines predicted or reported¹⁴ to be associated with MAP.

Residue	Reported Variant
C290	C290W ⁵⁵
C297	not reported
C300	not reported
C306	C306W (this study)
R241	R241W ^{53,55} , R241G ¹⁴
R245	R245L ⁵⁶ , R245C ¹⁴ , R245H ^{14,54}
R247	R247G ¹⁴
R309	R309C ^{9,57}

References

- 1) Nghiem, Y.; Cabrera, M.; Cupples, C. G.; Miller, J. H. The mutY gene: a mutator locus in *Escherichia coli* that generates G.C----T.A transversions. *Proc. Natl. Acad. Sci. USA* **1988**, *85*, 2709 – 2713.
- 2) Markkanen, E.; Dorn, J.; Hubscher, U. MUTYH DNA glycosylase: the rationale for removing undamaged bases from the DNA. *Front. Genet.* **2013**, *4*, 18.
- 3) Wallace, S. S.; Murphy, D. L.; Sweasy, J. B. Base excision repair and cancer. *Cancer Lett.* **2012**, *327*, 73 – 89.
- 4) Al-Tassan, N. *et al.* Inherited variants of MYH associated with somatic G:C-->T:A mutations in colorectal tumors. *Nature Genetics* **2002**, *30*, 227 – 232.
- 5) Nielsen, M.; Morreau, H.; Vasen, H. F.; Hes, F. J. MUTYH-associated polyposis (MAP). *Crit. Rev. Oncol. Hematol.* **2011**, *79*, 1 – 16.
- 6) Jasperson, K. W.; Tuohy, T. M.; Neklason, D. W.; Burt, R. W. Hereditary and familial colon cancer. *Gastroenterology* **2010**, *138*, 2044 – 2058.
- 7) Sampson, J. R. *et al.* Autosomal recessive colorectal adenomatous polyposis due to inherited mutations of MYH. *Lancet* **2003**, *362*, 39 – 41.
- 8) Wang, L. *et al.* MYH mutations in patients with attenuated and classic polyposis and with young-onset colorectal cancer without polyps. *Gastroenterology* **2004**, *127*, 9 – 16.
- 9) Sieber, O. M. *et al.* Multiple colorectal adenomas, classic adenomatous polyposis, and germ-line mutations in MYH. *N. Engl. J. Med.* **2003**, *348*, 791 – 799.
- 10) Isidro, G. *et al.* Germline MUTYH (MYH) mutations in Portuguese individuals with multiple colorectal adenomas. *Hum. Mutat.* **2004**, *24*, 353 – 354.
- 11) Cleary, S. P. *et al.* Germline MutY human homologue mutations and colorectal cancer: a multisite case-control study. *Gastroenterology* **2009**, *136*, 1251 – 1260.
- 12) Jones, N. *et al.* Increased colorectal cancer incidence in obligate carriers of heterozygous mutations in MUTYH. *Gastroenterology* **2009**, *137*, 489 – 494.
- 13) Farrington, S. M. *et al.* Germline susceptibility to colorectal cancer due to base-excision repair gene defects. *Am. J. Hum. Genet.* **2005**, *77*, 112 – 119
- 14) Out, A. A. *et al.* Leiden Open Variation Database of the MUTYH gene. *Hum. Mutat.* **2010**, *31*, 1205 – 1215.

- 15) Maio, N.; Rouault, T. A. Iron-sulfur cluster biogenesis in mammalian cells: New insights into the molecular mechanisms of cluster delivery. *Biochim. Biophys. Acta*, **2014**, *1853*, 1493 – 1512.
- 16) Alseth, I.; Eide, L.; Pirovano, M.; Rognes, T.; Seeberg, E.; Bjørås, M. The *Saccharomyces cerevisiae* homologues of endonuclease III from *Escherichia coli*, Ntg1 and Ntg2, are both required for efficient repair of spontaneous and induced oxidative damage in yeast. *Mol. Cell. Biol.* **1999**, *19*, 3779 – 3787.
- 17) Trasvina-Areñas, C. H.; Lopez-Castillo, L. M.; Sanchez-Sandoval, E.; Brieba, L. G. Dispensability of the [4Fe-4S] cluster in novel homologues of adenine glycosylase MutY. *FEBS J.* **2016**, *283*, 521 – 540.
- 18) Cunningham, R. P. *et al.* Endonuclease III is an iron-sulfur protein. *Biochemistry* **1989**, *28*, 4450 – 4455.
- 19) Porello, S. L.; Cannon, M. J.; David, S. S. A substrate recognition role for the [4Fe-4S]²⁺ cluster of the DNA repair glycosylase MutY. *Biochemistry* **1998**, *37*, 6465 – 6475.
- 20) Boal, A. K. *et al.* DNA-bound redox activity of DNA repair glycosylases containing [4Fe-4S] clusters. *Biochemistry* **2005**, *44*, 8397 – 8407.
- 21) Gorodetsky, A. A.; Boal, A. K.; Barton, J. K. Direct electrochemistry of endonuclease III in the presence and absence of DNA. *J. Am. Chem. Soc.* **2006**, *128*, 12082 – 12083.
- 22) Arnold, A. R.; Grodick, M. A.; Barton, J. K. DNA Charge Transport: from Chemical Principles to the Cell. *Cell Chem. Biol.* **2016**, *23*, 183 – 197.
- 23) O'Brien, E.; Silva, R. M.; Barton, J. K. Redox Signaling through DNA. *Isr. J. Chem.* **2016**, *56*, 705 – 723.
- 24) Yavin, E. *et al.* Protein-DNA charge transport: redox activation of a DNA repair protein by guanine radical. *Proc. Natl. Acad. Sci. USA* **2005**, *102*, 3546 – 3551.
- 25) Boal, A. K. *et al.* Redox signaling between DNA repair proteins for efficient lesion detection. *Proc. Natl. Acad. Sci. USA* **2009**, *106*, 15237 – 15242.
- 26) Miyoshi, Y. *et al.* Somatic mutations of the APC gene in colorectal tumors: mutation cluster region in the APC gene. *Hum. Mol. Genet.* **1992**, *1*, 229 – 233.
- 27) Donnelly, M. I. *et al.* An expression vector tailored for large-scale, high-throughput purification of recombinant proteins. *Protein Expr. Purif.* **2006**, *47*, 446 – 454.
- 28) Kapust, R. B.; Waugh, D. S. *Escherichia coli* maltose-binding protein is uncommonly effective at promoting the solubility of polypeptides to which it is fused. *Protein Sci.* **1999**, *8*, 1668 – 1674.

- 29) D'Agostino, V. G. *et al.* Functional analysis of MUTYH mutated proteins associated with familial adenomatous polyposis. *DNA Repair (Amst)* **2010**, *9*, 700 – 707.
- 30) Whicher, J. R. *et al.* Cyanobacterial polyketide synthase docking domains: a tool for engineering natural product biosynthesis. *Chemistry & Biology* **2013**, *20*, 1340 – 1351.
- 31) Kundu, S.; Brinkmeyer, M. K.; Livingston, A. L.; David, S. S. Adenine removal activity and bacterial complementation with the human MutY homologue (MUTYH) and Y165C, G382D, P391L and Q324R variants associated with colorectal cancer. *DNA Repair (Amst)* **2009**, *8*, 1400 – 1410.
- 32) Porello, S. L.; Leyes, A. E.; David, S. S. Single-turnover and pre-steady-state kinetics of the reaction of the adenine glycosylase MutY with mismatch-containing DNA substrates. *Biochemistry* **1998**, *37*, 14756 – 14764.
- 33) Rich, R. L.; Myszka, D. G. Higher-throughput, label-free, real-time molecular interaction analysis. *Anal. Biochem.* **2007**, *361*, 1 – 6.
- 34) Profrock, D.; Prange, A. Inductively coupled plasma-mass spectrometry (ICP-MS) for quantitative analysis in environmental and life sciences: a review of challenges, solutions, and trends. *Appl. Spectrosc.* **2012**, *66*, 843 – 868.
- 35) Pheaney, C. G.; Arnold, A. R.; Grodick, M. A.; Barton, J. K. Multiplexed electrochemistry of DNA-bound metalloproteins. *J. Am. Chem. Soc.* **2013**, *135*, 11869 – 11878.
- 36) Boon, E. M.; Salas, J. E.; Barton, J. K. An electrical probe of protein-DNA interactions on DNA-modified surfaces. *Nat. Biotechnol.* **2002**, *20*, 282 – 286.
- 37) Kelley, S. O.; Barton, J. K.; Jackson, N. M.; Hill, M. G. Electrochemistry of methylene blue bound to a DNA-modified electrode. *Bioconjug. Chem.* **1997**, *8*, 31 – 37.
- 38) Greeley, R. S.; Smith, W. T.; Stoughton, R. W.; Lietzke, M. H. Electromotive Force Studies in Aqueous Solutions at Elevated Temperatures .1. The Standard Potential of the Silver-Silver Chloride Electrode. *J. Phys. Chem-US* **1960**, *64*, 652 – 657.
- 39) Pope, M. A.; David, S. S. DNA damage recognition and repair by the murine MutY homologue. *DNA Repair (Amst)* **2005**, *4*, 91 – 102.
- 40) Johnson, M. K.; Duderstadt, R. E.; Duin, E. C. Biological and synthetic [Fe₃S₄] clusters. *Adv. Inorg. Chem.* **1999**, *47*, 1 – 82.
- 41) Sweeney, W. V.; Rabinowitz, J. C. Proteins containing 4Fe-4S clusters: an overview. *Annu Rev. Biochem.* **1980**, *49*, 139 – 161.

- 42) Duff, J. L. C.; Breton, J. L. J.; Butt, J. N.; Armstrong, F. A.; Thomson, A. J. Novel redox chemistry of [3Fe-4S] clusters: Electrochemical characterization of the all-Fe(II) form of the [3Fe-4S] cluster generated reversibly in various proteins and its spectroscopic investigation in *Sulfolobus acidocaldarius* ferredoxin. *J. Am. Chem. Soc.* **1996**, *118*, 8593 – 8603.
- 43) Netz, D. J. A. *et al.* Eukaryotic DNA polymerases require an iron-sulfur cluster for the formation of active complexes. *Nat. Chem. Biol.* **2012**, *8*, 125 – 132.
- 44) Good, N. E. *et al.* Hydrogen Ion Buffers for Biological Research. *Biochemistry* **1966**, *5*, 467 – 477.
- 45) Ugwu, S. O.; Apte, S. P. The Effect of Buffers on Protein Conformational Stability. *Pharmaceutical Technology* **2004**, *28*, 86 – 108.
- 46) O'Handley, S.; Scholes, C. P.; Cunningham, R. P. Endonuclease III interactions with DNA substrates. 1. Binding and footprinting studies with oligonucleotides containing a reduced apyrimidinic site. *Biochemistry* **1995**, *34*, 2528 – 2536.
- 47) O'Handley, S.; Scholes, C. P.; Cunningham, R. P. Endonuclease III interactions with DNA substrates. 1. Binding and footprinting studies with oligonucleotides containing a reduced apyrimidinic site. *Biochemistry* **1995**, *34*, 2528 – 2536.
- 48) Dorn, J.; Ferrarri, E.; Imhof, R.; Ziegler, N.; Hübscher, U. Regulation of human MutYH DNA glycosylase by the E3 ubiquitin ligase. *J. Biol. Chem.*, **2014**, *289*, 7049 – 7058.
- 49) Asso, M.; Guigliarelli, B.; Yagi, T.; Bertrand, P. EPR and redox properties of *Desulfovibrio vulgaris* Miyazaki hydrogenase: comparison with the Ni-Fe enzyme from *Desulfovibrio gigas*. *Biochim. Biophys. Acta* **1992**, *1122*, 50 – 56.
- 50) Teixeira, M. *et al.* Redox intermediates of *Desulfovibrio gigas* [NiFe] hydrogenase generated under hydrogen. Mossbauer and EPR characterization of the metal centers. *J. Biol. Chem.* **1989**, *264*, 16435 – 16450.
- 51) Kowal, A. T. *et al.* Effect of cysteine to serine mutations on the properties of the [4Fe-4S] center in *Escherichia coli* fumarate reductase. *Biochemistry* **1995**, *34*, 12284 – 12293.
- 52) Golinelli, M. P.; Chmiel, N. H.; David, S. S. Site-directed mutagenesis of the cysteine ligands to the [4Fe-4S] cluster of *Escherichia coli* MutY. *Biochemistry* **1999**, *38*, 6997 – 7007.
- 53) Bai, H. *et al.* Functional characterization of two human MutY homolog (hMYH) missense mutations (R227W and V232F) that lie within the putative hMSH6 binding domain and are associated with hMYH polyposis. *Nucleic Acids Res.* **2005**, *33*, 597 – 604.

- 54) Ali, M. *et al.* Characterization of mutant MUTYH proteins associated with familial colorectal cancer. *Gastroenterology* **2008**, *135*, 499 – 507.
- 55) Fleischmann, C. *et al.* Comprehensive analysis of the contribution of germline MYH variation to early-onset colorectal cancer. *Int. J. Cancer* **2004**, *109*, 554 – 558.
- 56) Bai, H. *et al.* Functional characterization of human MutY homolog (hMYH) missense mutation (R231L) that is linked with hMYH-associated polyposis. *Cancer Lett.* **2007**, *250*, 74 – 81.
- 57) Goto, M. *et al.* Adenine DNA glycosylase activity of 14 human MutY homolog (MUTYH) variant proteins found in patients with colorectal polyposis and cancer. *Hum. Mutat.* **2010**, *31*, E1861 – 1874.